Interfacial Phenomena and Heat Transfer, 12(1):51–61 (2024)

NUMERICAL STUDY OF THE EFFECT OF TUBE WALL ON SUBCOOLED BOILING AT THE END OF A LASER WAVEGUIDE

Viktor A. Kosyakov,[1,2,*] R.V. Fursenko,[1,2] S.S. Minaev,[2] & V.M. Chudnovskii[2]

[1]*Khristianovich Institute of Theoretical and Applied Mechanics, Siberian Branch of the Russian Academy of Science, Novosibirsk, Russia*

[2]*Institute of Applied Mathematics, Far Eastern Branch of the Russian Academy of Sciences, Vladivostok, Russia*

*Address all correspondence to: Viktor A. Kosyakov, Khristianovich Institute of Theoretical and Applied Mechanics, Siberian Branch of the Russian Academy of Science, Novosibirsk, Russia; Tel.: +79930252039; Fax: +73833307268, E-mail: asenya777@yandex.ru

Original Manuscript Submitted: 7/12/2023; Final Draft Received: 11/7/2023

Results of numerical simulations of the laser-induced boiling at the end of a waveguide placed inside the tube are presented. The effect of the tube wall on the vapor bubble evolution and characteristics of the cumulative jet forming as a result of its collapse was studied. Particularly, it was found that while the tubes of large radii insignificantly affect the velocity of the cumulative liquid jet, in the relatively narrow tubes the jet may not form at all. The effect of the tubes of moderate radii comes down to the decrease of the jet velocity compared to the case without the tube. A possible physical explanation of such influence of tube walls is proposed. Numerical results on laser-induced boiling inside the tubes are summarized in the regime diagram in the tube radius–waveguide radius plane.

KEY WORDS: *two-phase flow, vapor bubble, cumulative jet, subcooled boiling, compressibility, laser-induced boiling, CFD*

1. INTRODUCTION

A point-wise supply of heat to a liquid with a temperature of less than the saturation temperature can cause a process known as subcooled boiling (Tang et al., 2022; Wang et al., 2002). This process can be observed on thin wires and microheaters placed in a cold liquid. In contrast to the boiling of a liquid at saturation temperature, subcooled boiling is accompanied not only by the growing of vapor bubbles, but also by their collapse due to condensation. As a result, such phenomena as superintense nucleate boiling, thermal cavitation, etc., can be observed. In some cases, subcooled boiling may be accompanied by the formation of liquid or two-phase jets (Adamov et al., 2022; Chudnovskii et al., 2018). Despite their small size, the speed of such jets can reach hundreds of meters per second. Such jets are of great practical interest in various fields, for example, in laser micromachining of materials, submerged jets are used to create microreliefs on the surface of a material and to form microholes. In medicine, these jets can be used to perform surgical operations, and perforate, sanitize, and heat biological tissues (Yusupov and Chudnovskii, 2023). They also find technical applications in selective cleaning, treatment, and sanitation of surfaces. Thus, in engineering applications (Chahine et al., 2016), rapid bubble growth is an important mechanism for removing dirt particles, because there are strong suction forces around the rapidly growing bubble, which can create powerful forces to lift particles off the surface for cleaning. In medical applications (Ho et al., 2021), it is possible to use jets to destroy kidney calculi.

2169–2785/24/$35.00

The formation of liquid jets after the collapse of a gas or vapor bubble is a fairly well-known and actively studied phenomenon (Akhatov et al., 2001; Lu and Peng, 2007; Wang et al., 2002). A necessary condition for the jet formation after the collapse of a bubble in a liquid is the loss of bubble symmetry during its contraction. Adding a waveguide breaks the vertical symmetry that was present in free space without the waveguide. However, the symmetry in the dynamics of the bubble along the axis of symmetry of the waveguide is confirmed both by experimental data (Soyama, 2015) and by previous work done by other researchers (Yin et al., 2023). Thus, restrictions in the vicinity of the gas-vapor bubble contribute to the formation of the jet. The expansion and collapse of a bubble near a solid wall leads to the formation of a jet propagating toward the boundary, and when the bubble collapses near the free boundary, the jet is directed away from it.

The process of formation of a submerged jet in a configuration with a laser waveguide is described in Chudnovskii et al. (2020) and Fursenko et al. (2020). With the supply of laser radiation through the waveguide, the liquid near the waveguide endface is locally heated, which leads to liquid evaporation and the formation of a vapor bubble. Vapor overpressure associated with evaporation drives expansion of the vapor shell. After cessation of radiation, the bubble still expands by inertia for some time, thus entering a nonequilibrium state, i.e., the pressure inside the bubble becomes lower than the pressure of the surrounding liquid. After the bubble reaches its maximum volume, vapor condensation and reduced pressure lead to its rapid compression. As a result of almost complete condensation of the vapor and collapse of the bubble, a liquid jet of cumulative nature, directed from the end of the optical fiber toward the liquid, is formed.

Similar jets can also be observed in cavitation in various geometrical configurations, such as slits, holes, hollows, and other complex surface elements (Kauer et al., 2018). However, to date, the dynamics of a single bubble have been studied in the limited number of configurations, including solid boundaries and objects with a hole (Karri et al., 2011), blind holes (Trummler et al., 2020), parallel plates (Hsiao et al., 2013; Quah et al., 2018), pencil- and cylinder-shaped electrodes (Koch et al., 2021; Palanker et al., 2003), laser-induced boiling near a thin waveguide (Chudnovskii et al., 2017, 2018, 2020, 2021; Fursenko et al., 2020; Kosyakov et al., 2022; Levin et al., 2022).

The latter configuration is the focus of the present study. In Fursenko et al. (2020), the effect of the waveguide size on the cumulative jet velocity was investigated numerically. The results showed that, for a given bubble radius, there is an optimal fiber radius at which the average jet velocity is maximal. Numerical simulations within the framework of an incompressible mathematical model (Kosyakov et al., 2022) showed that the jet velocity can be significantly affected by solid walls located near the optical fiber. Depending on the geometric configuration of the walls, the average jet velocity can either increase compared to the case when there are no walls or decrease up to zero. Chudnovskii et al. (2020) showed that a bubble collapse stage of laser-induced boiling can be followed by series of rebounds manifested in secondary expansion of the bubble after its contraction.

In the previously cited numerical papers on laser-induced boiling, either the compressibility of the medium was not taken into account or the growth and collapse of the bubble were considered as two separate stages, resulting in incomplete accounting of an interplay between these stages. Although such approximations have been justified in the case of the laser-induced boiling in free space by satisfactory agreement between numerical results and experimental data (Chudnovskii et al., 2020; Levin et al., 2022), the applicability of an incompressible mathematical model in the presence of solid walls near the waveguide is still an open question.

The main objective of this paper is to study the effect of tube walls on the evolution of the vapor bubble and characteristics of the cumulative jet during the laser-induced boiling by means of compressible numerical calculations. These calculations will contribute to the understanding of the impact of the compressibility on the process and make it possible to determine the limits of applicability of the incompressible model.

2. MATHEMATICAL MODEL

In the axisymmetric configuration shown in Fig. 1, we consider laser-induced subcooled boiling near the tip of a laser waveguide immersed in a liquid. The radius of the waveguide, R_f = 300 μm, was the same for all calculations. The tube radius, R_t, was varied from 1.5 to 50 waveguide calibers. At the external boundaries of the computational domain (dashed lines), the constant pressure conditions $p = p_0 + 0.5\rho U^2)$ with $p_0 = 10^5$ Pa are imposed and no-slip conditions $(\overrightarrow{U} = 0, \partial P/\partial n = 0)$ are set on the waveguide surface (solid lines). Mass transfer across the

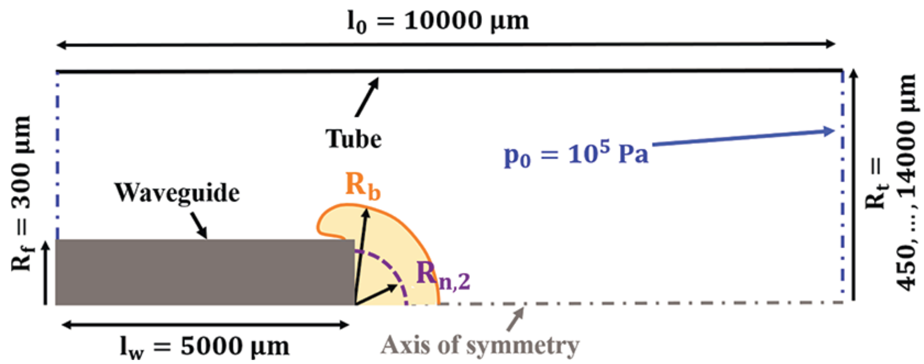

FIG. 1: Scheme of computation domain

gas–liquid interface, gravitational force, and surface tension are neglected (Koch et al., 2021). The energy equation can be omitted because the gas is assumed to be perfect, adiabatic, and compressible (the dependence of density on pressure and does not take temperature into account). Compressibility of the liquid is neglected.

The equations for two-phase flow according to these assumptions and using the volume of fluid (VOF) method (de Niem et al., 2007) are as follows:

Continuity equation:

$$\frac{\partial \rho_g \alpha_g}{\partial t} + \nabla(\rho_g \alpha_g \vec{U}) = \dot{\rho}_{g,m}, \quad \frac{\partial \rho_l \alpha_l}{\partial t} + \nabla(\rho_l \alpha_l \vec{U}) = 0, \quad \rho = \rho_l \alpha_l + \rho_g \alpha_g, \tag{1}$$

Momentum equation:

$$\frac{\partial \rho \vec{U}}{\partial t} + \nabla(\rho \vec{U}\vec{U}) = -\nabla p + \nabla \left[\mu \left(\nabla \vec{U} + \left(\nabla \vec{U} \right)^T \right) - \frac{2}{3} \left(\nabla \vec{U} \right) I \right], \tag{2}$$

Equations of state:

$$\rho_g = \rho_{g,0} \left(\frac{p_g}{p_{g,0}} \right)^{1/\gamma_g}, \quad \rho_l = \text{const}, \tag{3}$$

where α_g and α_l are volume fractions introduced to distinguish between liquid and gas phases, which are denoted by the subscripts (l) and (g), respectively, in Eqs. (1)–(3). The values of $\alpha_{g,s}$ range from 0 to 1, with $\alpha_g + \alpha_l = 1$ everywhere in the computational domain. For the liquid phase $\alpha_l = 1$, $\alpha_g = 0$, and for the gas phase $\alpha_l = 0$, $\alpha_g = 1$; I – identity matrix; $p_{g,0}$ and $\rho_{g,0}$, the pressure and density of the gas in the bubble of equilibrium radius R_n at normal conditions; γ_g – adiabatic index.

Algebraic relations are used to determine the total fields ρ and μ in Eqs. (1)–(3), as follows:

$$\rho = \alpha_g \rho_g + \alpha_l \rho_l, \qquad \mu = \alpha_g \mu_g + \alpha_l \mu_l, \tag{4}$$

and kinematic viscosity for gas and liquid are $\nu_g = 1.8 \times 10^{-5}$ and $\nu_l = 3.65 \times 10^{-4}$ m^2/s, respectively.

According to Koch et al. (2021), a linear increase and decrease of the equilibrium equivalent radius (R_n) of the vapor bubble is used to model the processes of evaporation and condensation, as follows:

$$R_n(t) = \begin{cases} R_{n,1}, \ t < t_a \\ (t - t_a) \cdot \frac{R_{n,2} - R_{n,1}}{t_b - t_a} + R_{n,1}, \ t_a \le t < t_b \\ R_{n,2}, \ t \ge t_b \end{cases}, \tag{5}$$

where t_a is the time moment of the beginning of the evaporation or condensation process; t_b is the time when evaporation or condensation stops, $R_{n,1}$ is the initial bubble radius, $R_{n,2}$ is the final radius reached in the equilibrium process. The cases with $R_{n,1} < R_{n,2}$ correspond to evaporation, and for condensation $R_{n,1} > R_{n,2}$. The mass and density of a bubble of radius $R_n(t)$ in the equilibrium state are defined as follows:

$$m_{0,new} = m_0 \left(\frac{R_n(t)}{R_{n,1}} \right)^3, \quad \rho_{g,new}(x,t) = \frac{m_{0,new}}{m(t)} \rho_g(x,t), \tag{6}$$

where m_0 is the mass of the bubble at radius $R_{n,1}$, $m_{0,new}$ is the new mass of the bubble at the new time step, and $m(t)$ is the mass of the bubble at the current time step. Thus, evaporation or condensation is reduced to an increase or decrease in the gas content of the bubble according to the Eqs. (5) and (6).

This empirical approach has been proposed and tested in Koch et al. (2021) as an application to condensation modeling. The phenomenon of laser-induced breakdown with bubble formation is not modeled in this work. Instead, an initial bubble is taken and by evaporation, which is modeled by increasing the bubble radius R_n, and the bubble is expanded to the experimental maximum radius. Condensation of the vapor part of the bubble is modeled by decreasing the radius of the bubble R_n. The shape and size of the bubble as a function of time were found to be in good agreement with the experimental data, these results can be found in our previous work (Kosyakov et al., 2023).

The initial bubble radius was $R_{b,0} = 50$ μm. In all calculation cases presented next, the evaporation model was run at the start of the calculation and its parameters were $t_b - t_a = 210$ μs and $R_{n,2} = 1550$ μm. When the bubble reached its maximum volume, the condensation model was started at the following parameters $t_b - t_a = 10 \times 10^2$ μs and $R_{n,2} = 50$ μm. The parameters were chosen based on the evolution of the bubble in the experiments shown in Fig. 2.

The finite volume method implemented in the OpenFOAM (Weller et al., 1998) software was used to numerically solve the Eqs. (1)–(3). The CompressibleInterFoam solver was modified to compute a correction for the gas phase density in accordance with the evaporation/condensation model [Eqs. (5) and (6)]. The supplementary materials contain the part of code responsible for the phase change (ModComInterFoam.zip). To investigate grid convergence, a series of calculations on meshes with a gradual decrease in mesh size was carried out. Uniform orthogonal meshes were considered. They were equally spaced radially and axially at intervals of 15, 10, 8, 6, and 5 μm. Numerical tests showed that the instantaneous velocities along the symmetry axis differed by $<$ 5% for 6 and 5 μm meshes. The 6 μm mesh was therefore used for all further calculations.

3. RESULTS AND DISCUSSION

The main geometrical parameters characterizing the laser-induced boiling inside the tube are the waveguide radius (R_f) and tube radius (R_t). Both these parameters were scaled by the equivalent bubble radius at the peak of its expansion ($R_{b,\max}$), which is related with the energy fed in the system. The equivalent bubble radius was calculated from the volume of the gas phase, assuming that it is spherical. The ranges of variation of nondimensional geometrical parameters are $\overline{R_f} = R_f/R_{b,\max} = 0.15, \ldots, \infty$ and $\overline{R_t} = R_t/R_{b,\max} = 0.8, \ldots, \infty$.

The limiting case of $\overline{R_t} = \infty$, $\overline{R_f} \to \infty$, corresponds to the bubble collapse near the infinite plate. In this case, which is widely known and described in many works, the collapsing bubble forms a jet directed toward the plate. The velocity of such a jet can reach hundreds of meters per second (Lechner et al., 2023).

When the waveguide radius is reduced to $\overline{R_f} \approx 1$, there is a transition to the case of bubble collapse at the end of the waveguide in free space. In this case, in the course of the bubble contraction, a convergent liquid jet directed toward the symmetry axis is formed. This jet cuts through the bubble and collides with itself on the axis of symmetry forming the cumulative jet directed away from the waveguide into free space.

Further reduction of the dimensionless radius of the waveguide causes the bubble to envelop part of the waveguide during expansion stage, thereby taking the form of a mushroom cap. This change in the shape of the vapor bubble does not significantly affect the mechanism of its collapse and velocity of the cumulative jet. Figure 2 shows the evolution of the vapor bubble and subsequent jet formation typical for $\overline{R_f} \lesssim 1$ and $\overline{R_t} = \infty$. The right part of each snapshot corresponds to the experimental data obtained by using high-speed filming, while the left half of each frame is the simulation result calculated for $\overline{R_f} = 0.15$. In unbounded space, the expanding bubble retains a spherical shape. During the bubble collapse, it loses symmetry but the process itself is symmetrical with respect to the rotational axis.

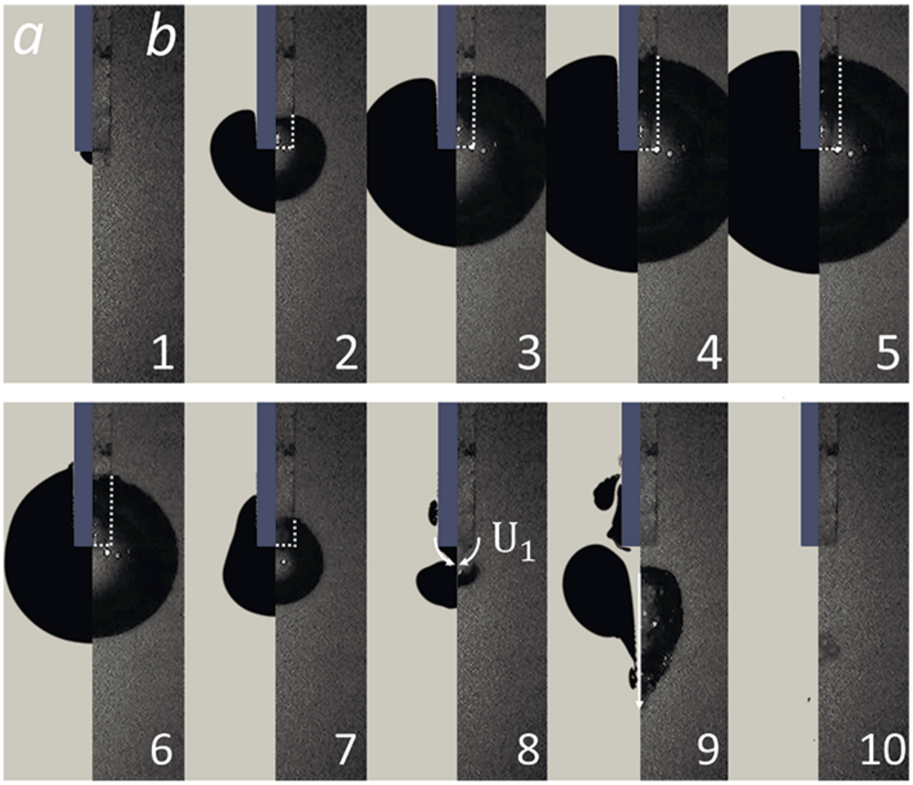

FIG. 2: Evolution of a vapor bubble at the end of a waveguide in unbounded space obtained experimentally (right half of each snapshot) and numerically (left half) for $\overline{R_t} = \infty$, $\overline{R_f} = 0.15$. Time interval between the frames is 60 μs.

The convergent jet with velocity U_1 collides on the symmetry axis as demonstrated by frame 8 in Fig. 2. As a result of this collision of the oncoming liquid flows, a cumulative jet directed away from the end of the waveguide is formed (frame 9). Then there is a rebound, which is clearly visible in frames 9 and 10, as the repeated growth of the bubble, and finally it completes dissipation.

Chudnovskii et al. (2020) suggested that the characteristics of the cumulative jet are mainly defined by the velocity and angle of the convergent liquid jet. The mechanism of cumulative jet formation proposed by Chudnovskii et al. (2020) and confirmed by numerical simulations (Fursenko et al., 2020) is schematically shown in Fig. 3. Velocity and the angle of the convergent jet are denoted in Fig. 3 as U_1 and ϕ, correspondingly. In these notations, the estimate of the velocity of cumulative jet (Chudnovskii et al., 2020) reads

$$U_{jet} = U_1(1 + \cos\phi)/\sin\phi. \tag{7}$$

All abovementioned discussion concerned the laser-induced boiling in the unbounded space; that is $\overline{R_t} = \infty$. However if the process takes place inside the tube, the inflow of a liquid from the radial direction is limited by walls. This affects the velocity vector U_1, and as a consequence, the cumulative jet characteristics. To evaluate the effect of the tube, we fixed the dimensionless waveguide radius $\overline{R_f} = 0.15$ and gradually decreased the tube radius $\overline{R_t}$. Figure 4 shows liquid flow stream lines calculated for the cases with $\overline{R_t} = 2.5$ (left half of each frame) and $\overline{R_t} = 3.25$ (right half).

In the first two frames of Fig. 4, the bubbles inside the tubes of different radii expand identically and reach their maximum size at ~ 400 μs. Thus, the bubble expansion stage inside the tube takes longer than in the free space (see Fig. 2). At the collapse stage, the tube wall restricts the liquid inflow from the radial direction, while there are no restrictions for the axial flow. As a result, the bubble contraction in the direction perpendicular to the tube wall slows down compared to the direction parallel to the wavegude. For example, in the free space and wide tubes ($\overline{R_t} > 5$)

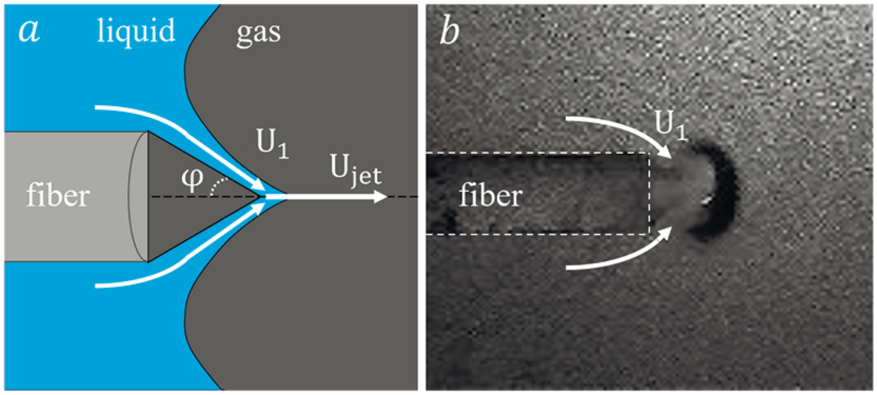

FIG. 3: Mechanism of jet formation due to the collision of convergent liquid jet on the symmetry axis: (a) schematic representation and (b) experiment

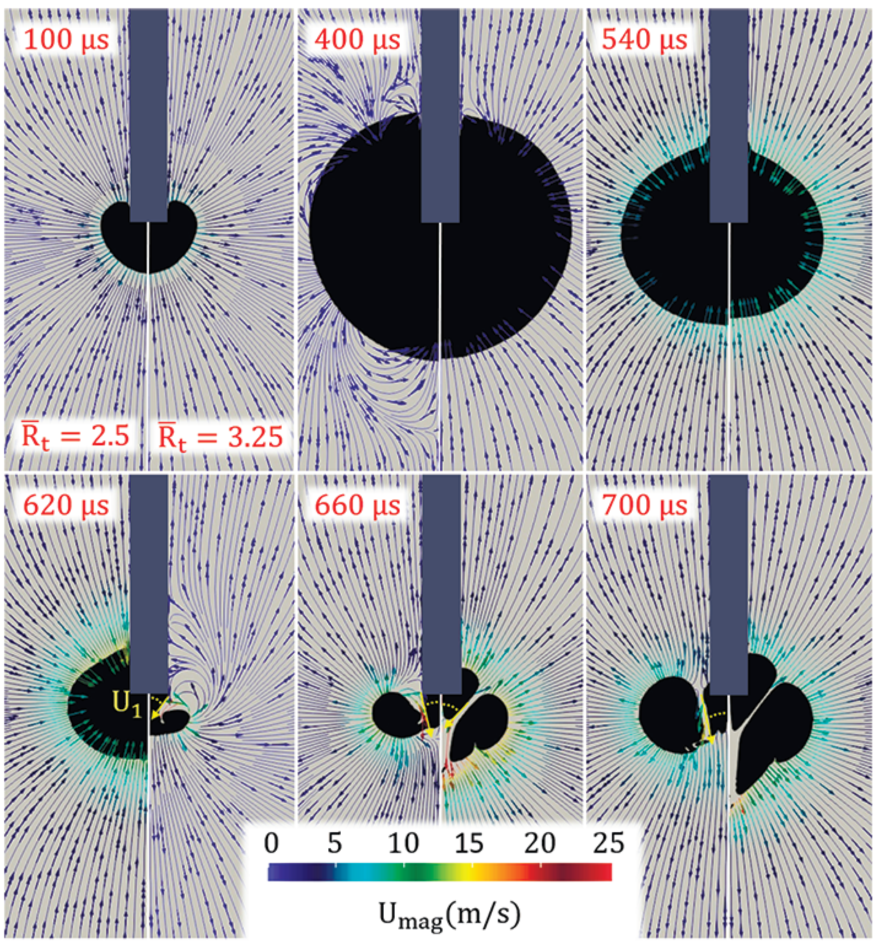

FIG. 4: Evolution of a vapor bubble and liquid flow streamlines inside the tubes of non-dimensional radii $\overline{R_t} = 2.5$ (left half of each frame) and $\overline{R_t} = 3.25$ (right half). Detailed vapor bubble evolutions are given in the supplemental materials for the left case (see Supplementary Movie 1) and for the right case (see Supplementary Movie 2).

the average ratio of bubble sizes in axial D_z and radial D_r directions at the collapse stage is close to unity. With narrowing of the tube, this ratio gradually decreases and $D_z/D_r = 0.82$, 0.56, and 0.25, for $\overline{R_t} = 3.25$, 2.5, and 1.75, correspondingly. For narrow tubes $\overline{R_t} < 1.2$, the bubble contracts only in the direction parallel to the waveguide, while the change of its size in the perpendicular direction is negligible. Thus, $D_z/D_r \to 0$ during the bubble collapse stage.

Noticeable differences are also observed in the velocity and direction of the convergent jet. In the narrow tube, the angle ϕ between the vector U_1 and symmetry axis decreases. In free space (frame 8 in Fig. 2), the angle ϕ is $\sim$ 45 deg, while in the relatively wide tube $\overline{R_t} = 3.25$ it becomes to be $\sim$ 38 deg [time 620 μs in Fig. 4(right)]. Numerical simulations showed that, in this case the velocity of the cumulative jet is less than in the free space (50 m/s against 73 m/s) in agreement with theoretical predictions (Chudnovskii et al., 2020). With the decrease of the tube radius, the angle ϕ decreases and for $\overline{R_t} = 2.5$ it is 16 deg [time 660, 700 μs in Fig. 4(left)]. At such a small angle, the convergent jet breaking through the bubble collides with the liquid on the opposite side of the bubble, as is shown in Fig. 4, time 660, 700 μs, rather than collapses at the symmetry axis. As a result, a cumulative jet is not formed in this case. The decrease of the angle ϕ is associated with the rebound manifested in the secondary expansion of the residual of the vapor bubble, which leads to the rejection of the convergent jet aside (see Fig. 4, time 660, 700 μs).

It is worth noting that previous numerical studies in the framework of an incompressible gas model intimated that the jet is formed inside the tube regardless of its radius. The only difference between the dynamics of incompressible and compressible bubbles explaining this contradiction is the rebound. Comparison of the bubbles' shapes and the liquid flow streamlines obtained by using these two models showed that, in the compressible case the angle ϕ is less due to the deflection of the convergent jet by the rebounding vapor pocket seen in Fig. 4 time 700 μs. The reader can find additional results comparing the incompressible and compressible models in the supplementary materials (see Supplementary Fig. 2, Supplementary Movies 3 and 4).

Figure 5 shows the dependency of the velocity of the cumulative jet (U_{jet}) on the non-dimensional tube radius ($\overline{R_t}$). In the wide tubes U_{jet} is almost independent on tube radius since the walls effect on flow dynamics is minor. With the decrease of $\overline{R_t}$, the jet velocity is reduced due to the above-discussed reasons, briefly, the speed drops due to a change in the angle of the converging fluid flow ϕ, which, upon collision on the axis of symmetry, forms a cumulative jet. Finally, in enough narrow tubes the jet is not formed at all (this is designated as $U_{jet} = 0$ in Fig. 5). The dashed line in Fig. 5 corresponds to the theoretical estimation (7) of the velocity of the cumulative jet proposed in Chudnovskii et al. (2020). The values of U_1 and ϕ in Eq. (7) were taken from the simulations. For tubes of large and moderate radii, a simple estimate (7) agrees well with the numerical results. For the narrow tubes ($\overline{R_t} < 3.25$),

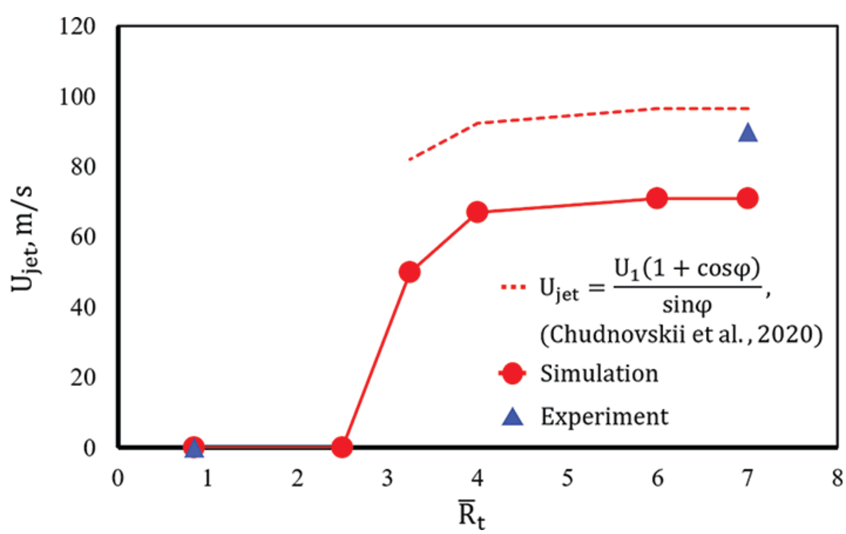

FIG. 5: Dependencies of the jet velocity on the dimensionless tube radius obtained by using analytical estimation (7) (dashed line), numerically (solid line), and experimentally (triangles)

theory predicts finite values of jet velocity while the numerical simulations indicate impossibility of the jet formation. This discrepancy is due to the theoretical assumption that the vapor bubble is large enough so that the convergent jet cutting through the bubble collapsed at the symmetry axis. Numerical simulations showed that at small tube radii this assumption is not valid because convergent flow of small angle ϕ bursts the bubble and collides with the liquid on the other side of it, as demonstrated in Fig. 4, time 700 μs. It should also be noted that numerical results agree with available experimental data depicted in Fig. 5 by triangles. In a wide tube, the error in the velocity of the cumulative jet between the analytical and experimental data, as well as the analytical and numerical data, is 8 and 20%, respectively. In a narrow tube, the analytical solution was not considered due to the inability to capture the effect of compressibility, the error between the experimental and numerical results is 0% (no jets).

The experimental data on laser-induced boiling in the quartz tubes (Chudnovskii et al., 2023) confirm the obtained numerical results. Figure 6 shows evolution of the bubble shape in the tube of radius $\overline{R_t} = 0.8$, obtained numerically (left half of each frame) and experimentally (right half) by using high-speed filming. Figure 6 clearly demonstrates the above mentioned numerical result predicting preferential contraction of the bubble in the axial direction inside the narrow tubes. Numerical results well coincides with experiments in characteristic times of the process and bubble shape, except the part enveloping waveguide. This difference may be accounted with boundary conditions, because in experiments the liquid volume is finite and its boundaries may affect the process. Both experiments and simulations showed the appearance of the cone-shaped cap at the bubble surface near the symmetry axis (see frames 700–950 μs in Fig. 6). As the bubble is shrunk, the tip of this cap moves toward the waveguide endface.

Experimentally and numerically determined velocities of the bubble surface on the symmetry axis (U_x) at expansion and collapse stages are shown in Fig. 7 and demonstrate good agreement, the difference in speeds on average being $< 15\%$. The velocity of boundary motion at the phase boundary was calculated as follows. In the experiment, the $x(t)$ dependence was obtained from the frames of the experiment captured by a high-speed camera, and then the $U(t)$ dependence was obtained by differentiation. In numerical modeling, these data are obtained based on the volume of fluid (VoF) method. During the bubble expansion stage, the velocity U_x is positive and slows down to zero by the time when the bubble reaches is maximum volume. Then, the bubble collapses with acceleration and velocity of the cap tip propagation is negative.

All regimes of laser-induced boiling discussed earlier can be summarized in a diagram plotted in the tube radius–waveguide radius plane. Such a diagram in non-dimensional coordinates $\overline{R_t}$ and $\overline{R_f}$ is shown in Fig. 8. In the right part of this diagram, R_t tends to infinity which corresponds to the bubble collapse in free space, previously considered in Fursenko et al. (2020) and Kosyakov et al. (2022). Evolution of the bubble shape typical for this case is illustrated by Fig. 2. Bubble collapse near the tip of the waveguide in this case results in formation of a cumulative jet. Another limiting case is placed in the top right corner of the diagram ($\overline{R_t} \gg \overline{R_f} \to \infty$, top right region in Fig. 8) and corresponds to the bubble collapse near the infinite plate. This case has been described in Lechner et al. (2023) and is characterized by formation of the liquid jet directed toward the plate. For these two limiting cases, the effect of tube wall is negligible. With the decrease of the tube radius ($\overline{R_t}$) (bottom right region), the presence of the tube starts

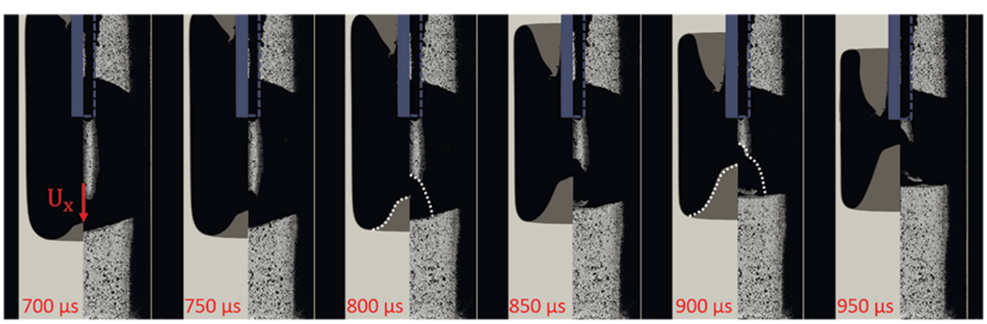

FIG. 6: Evolution of the bubble shape during laser-induced boiling for $\overline{R_t}$ = 0.8 and $\overline{R_f}$ = 0.15, obtained experimentally (right half of each frame) and numerically (left half). Time between frames was 50 μs. A detailed evolution of the vapor bubble is given in Supplementary Fig. 1.

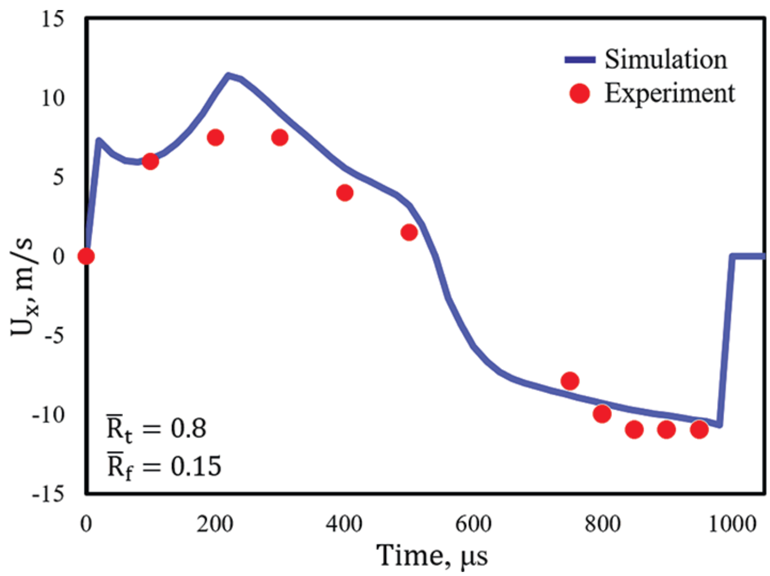

FIG. 7: Temporal dependencies of phase interface velocity at the symmetry axis obtained numerically and by post-processing of experimental results for the case shown in Fig. 6

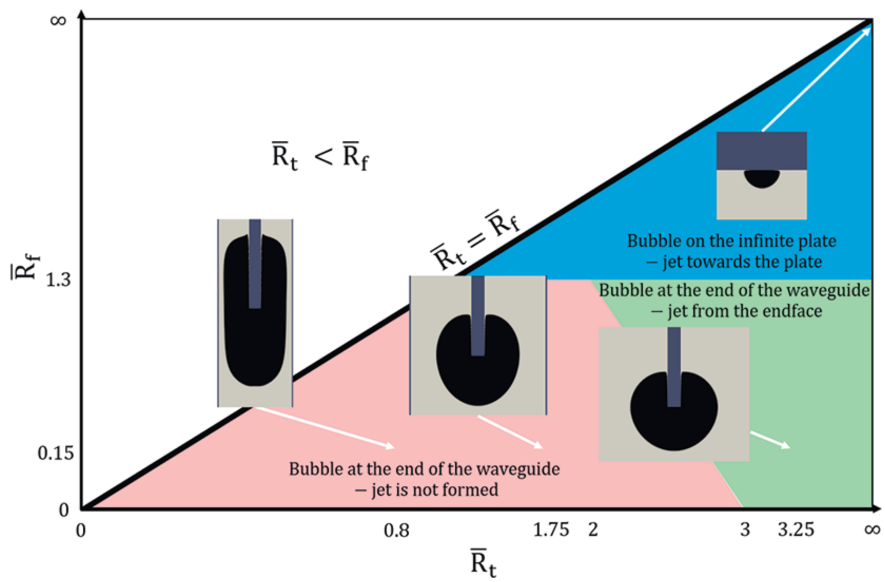

FIG. 8: Non-dimensional regime diagram in the tube radius–waveguide radius plane

to affect the bubble dynamics. This case is illustrated by the right half of frames in Fig. 4. Although the flattening of the bubble in the axial direction at the contraction stage becomes notable, an intensive cumulative jet forms after its collapse. With further decrease of the tube radius, the influence of the walls becomes more pronounced, which is manifested in significant contraction of the bubble in the direction parallel to the waveguide. As a result, the bubble collapse no more leads to the formation of the cumulative jet. The range of parameters corresponding to this regime is depicted in Fig. 8 by the bottom left region. Dynamics of the bubble and the liquid flow streamlines typical for this regime are shown in left half of the frames in Figs. 4 and 6.

4. CONCLUSIONS

Numerical simulations of the evolution of a single vapor bubble near the tip of a laser waveguide in a tube have yielded data on the effect of tube and waveguide dimensions on the flow fields and characteristics of the cumulative jet.

1. The process of a vapor bubble collapse during laser-induced boiling depends on non-dimensional radius ($\overline{R_t}$) of the waveguide normalized by maximum bubble radius. For $1.3 < \overline{R_t} < \infty$, the process coincides with the classical case of bubble collapse near an infinite plate. In this case, the liquid jet forming as a result of bubble collapse is directed towards the plate along the normal. If the value of the dimensionless waveguide radius is approximately equal to unity, the bubble radius is close to the waveguide radius and the jet is directed away from the waveguide end face. For the values of the non-dimensional radius of the waveguide less than unity, the bubble takes the form of a mushroom cap, while the jet is also directed from the end of the waveguide.

2. The placement of the waveguide inside the tube can affect the bubble evolution and the process of cumulative jet formation. For the infinite plate case $\overline{R_f} > 1.3$, the tube does not introduce any significant changes in the process. However, for the dimensionless waveguide radii of < 1.3, the jet is not formed in tubes narrower than $\overline{R_t} < 2, \ldots, 3$ depending on the waveguide radius.

3. The absence of the cumulative jet in the narrow tubes, showed numerically and confirmed experimentally, is explained by rebound. Re-expansion expansion of the bubble leads to a change in the velocity vector of the convergent liquid flow, in such a way that it is not self-collides on the symmetry axis, which is a necessary condition for the formation of a cumulative jet. Since the rebound can be captured only in the framework of the compressible model, compressibility should be taken into account in the case of simulations in the narrow tubes, while in the wide tubes this effect may be not so prominent.

4. The theoretical estimate of cumulative jet velocity proposed by Chudnovskii et al. (2020) based on the velocity and angle of converging fluid flow agrees well with the numerical results for wide tubes $\overline{R_t} \geq 3.25$. However, this estimate cannot be used for smaller tubes because of the violation of assumption that the bubble size is large enough for the fluid flow to converge on the axis of symmetry.

ACKNOWLEDGMENT

This work was supported by the Russian Science Foundation (Project No. 22-19-00189).

REFERENCES

Adamov, T., Chudnovsky, V., and Elistratov, D., Spontaneous (Spontaneous) Boiling of Submerged Jets, Generated during the Collapse of Vapor Bubbles, *Tech. Phys. Lett.*, vol. **1**, p. 16, 2022.

Akhatov, I., Lindau, O., Topolnikov, A., Mettin, R., Vakhitova, N., and Lauterborn, W., Collapse and Rebound of a Laser-Induced Cavitation Bubble, *Phys. Fluids*, vol. **13**, no. 10, pp. 2805–2819, 2001.

Chahine, G.L., Kapahi, A., Choi, J.K., and Hsiao, C.T., Modeling of Surface Cleaning by Cavitation Bubble Dynamics and Collapse, *Ultrason. Sonochem.*, vol. **29**, pp. 528–549, 2016.

Chudnovskii, V.M., Yusupov, V.I., Dydykin, A.V., Nevozhai, V.I., Kisilev, A.Y., Zhukov, S.A., and Bagratashvili, V.N., Laser-Induced Boiling of Biological Liquids in Medical Technologies, *Quantum Electron.*, vol. **47**, no. 4, pp. 361–370, 2017.

Chudnovskii, V., Mayor, A., Kiselev, A., and Yusupov, V., Foaming of Blood in Endovenous Laser Treatment, *Lasers Med. Sci.*, vol. **33**, no. 8, pp. 1821–1826, 2018.

Chudnovskii, V., Levin, A., Yusupov, V., Guzev, M., and Chernov, A., The Formation of a Cumulative Jet during the Collapse of a Vapor Bubble in a Subcooled Liquid Formed as a Result of Laser Heating, *Int. J. Heat Mass Transf.*, vol. **150**, p. 119286, 2020.

Chudnovskii, V., Guzev, M., Yusupov, V., Fursenko, R., and Okajima, J., Study of Methods for Controlling Direction and Velocity of Liquid Jets Formed during Subcooled Boiling, *Int. J. Heat Mass Transf.*, vol. **173**, p. 121250, 2021.

Chudnovskii, V., Guzev, M., Dats, E., and Kulik, A., The Effect of Accelerated Intake of Liquid in the Tube during Laser Cavitation on a Laser Heating Element, *Dokl. Phys.*, Submitted 2023. DOI: 10.1016/j.ijheatmasstransfer.2019.119286

de Niem, D., Kuhrt, E., and Motschmann, U., A Volume-of-Fluid Method for Simulation of Compressible Axisymmetric Multi-Material Flow, *Comput. Phys. Commun.*, vol. **176**, no. 3, pp. 170–190, 2007.

Fursenko, R., Chudnovskii, V., Minaev, S., and Okajima, J., Mechanism of High Velocity Jet Formation after a Gas Bubble Collapse near the Micro Fiber Immersed in a Liquid, *Int. J. Heat Mass Transf.*, vol. **163**, p. 120420, 2020.

Ho, D., Scialabba, D., Terry, R., Ma, X., Chen, J., Sankin, G., Gaoming, X., Qi, R., Preminger, G., Lipkin, M., and Zhong, P., The Role of Cavitation in Energy Delivery and Stone Damage during Laser Lithotripsy, *J. Endourol.*, vol. **35**, pp. 860–870, 2021.

Hsiao, C.T., Choi, J.K., Singh, S., Chahine, G.L., Hay, T.A., Ilinskii, Y.A., Zabolotskaya, E.A., Hamilton, M.F., Sankin, G., Yuan, F., and Zhong, P., Modelling Single- and Tandem-Bubble Dynamics between Two Parallel Plates for Biomedical Applications, *J. Fluid Mech.*, vol. **716**, pp. 137–170, 2013.

Karri, B., Pillai, K.S., Klaseboer, E., Ohl, S.W., and Khoo, B.C., Collapsing Bubble Induced Pumping in a Viscous Fluid, *Sens. Actuators A*, vol. **169**, no. 1, pp. 151–163, 2011.

Kauer, M., Belova-Magri, V., Cairos, C., Linka, G., and Mettin, R., High-Speed Imaging of Ultrasound Driven Cavitation Bubbles in Blind and through Holes, *Ultrason. Sonochem.*, vol. **48**, pp. 39–50, 2018.

Koch, M., Rossello, J., Lechner, C., Lauterborn, W., and Mettin, R., Dynamics of a Laser-Induced Bubble above the Flat Top of a Solid Cylinder—Mushroom-Shaped Bubbles and the Fast Jet, *Fluids*, vol. **7**, p. 2, 2021.

Kosyakov, V., Zakharov, A., and Fursenko, R., Numerical Study of the Solid Walls Effect on the Velocity of a Liquid Jet Formed as the Result of Vapor Bubble Collapse near a Rod, *Far East Math. J.*, vol. **22**, pp. 185–189, 2022.

Kosyakov, V.A., Fursenko, R.V., Chudnovskii, V.M., and Minaev, S.S., Physical Mechanisms Controlling a Vapor Bubble Collapse and Formation of a Liquid Jet during a Laser-Induced Subcooled Boiling near the End Face of a Thin Waveguide, *Int. Commun. Heat Mass Transf.*, vol. **148**, p. 107053, 2023.

Lechner, C., Koch, M., Lauterborn, W., and Mettin, R., Fast Jets from Bubbles Close to Solid Objects: Examples from Pillars in Water to Infinite Planes in Different Liquids, *Tech. Mech.*, vol. **43**, pp. 21–37, 2023.

Levin, A., Chernov, A.A., and Safarov, A., Formation Mechanism of a Cumulative Jet Resulting from the Collapse of a Laser-Induced Vapor Bubble in a Subcooled Liquid, *SSRN Electron. J.*, 2022. DOI: 10.2139/ssrn.4218426

Lu, J. and Peng, X., Bubble Jet Flow Formation during Boiling of Subcooled Water on Fine Wires, *Int. J. Heat Mass Transf.*, vol. **50**, no. 19, pp. 3966–3976, 2007.

Palanker, D., Vankov, A., Miller, J., Friedman, M., and Strauss, M., Prevention of Tissue Damage by Water Jet during Cavitation, *J. Appl. Phys.*, vol. **94**, no. 4, pp. 2654–2661, 2003.

Quah, E.W., Karri, B., Ohl, S.W., Klaseboer, E., and Khoo, B.C., Expansion and Collapse of an Initially Off-Centered Bubble within a Narrow Gap and the Effect of a Free Surface, *Int. J. Multiphase Flow*, vol. **99**, pp. 62–72, 2018.

Soyama, H., Surface Mechanics Design by Cavitation Peening, *J. Eng.*, vol. **2015**, no. 13, pp. 110–114, 2015.

Tang, J., Hu, R., Liu, H., Mo, Z., and Sun, L., Numerical Investigation of Thermally Controlled Bubble Condensation near a Solid Wall, *Chem. Eng. Sci.*, vol. **262**, p. 118018, 2022.

Trummler, T., Bryngelson, S.H., Schmidmayer, K., Schmidt, S.J., Colonius, T., and Adams, N.A., Near-Surface Dynamics of a Gas Bubble Collapsing above a Crevice, *J. Fluid Mech.*, vol. **899**, p. A16, 2020.

Wang, H., Peng, X., Wang, B., and Lee, D., Jet Flow Phenomena during Nucleate Boiling, *Int. J. Heat Mass Transf.*, vol. **45**, no. 6, pp. 1359–1363, 2002.

Weller, H.G., Tabor, G., Jasak, H., and Fureby, C., A Tensorial Approach to Computational Continuum Mechanics Using Object-Oriented Techniques, *Comput. Phys.*, vol. **12**, no. 6, pp. 620–631, 1998.

Yin, J., Zhang, Y., Gong, D., Tian, L., and Du, X., Dynamics of a Laser-Induced Cavitation Bubble near a Cone: An Experimental and Numerical Study, *Fluids*, vol. **8**, p. 220, 2023.

Yusupov, V. and Chudnovskii, V., The Origin of Loud Claps during Endovenous Laser Treatments, *J. Acoust. Soc. Am.*, vol. **153**, no. 3, pp. 1525–1533, 2023.